Journal of Nanostructure in Chemistry
https://doi.org/10.1007/s40097-021-00424-7

ORIGINAL RESEARCH

Facile synthesis of reduced graphene oxide aerogel in soft drink as supercapacitor electrode

Yasin M. Y. Albarqouni[1] · Soon Poh Lee[1] · Gomaa A. M. Ali[2] · Anita Sagadevan Ethiraj[3] · H. Algarni[4,5] · Kwok Feng Chong[1]

Received: 8 January 2021 / Accepted: 8 July 2021

Abstract
A facile approach is reported to produce reduced graphene oxide (rGO) aerogel. The proposed approach involves the reduction of GO by utilizing the reduction capability of carbonic acid in soft drinks. The presence of carbonic acid reduces the oxygen functionalities in GO to produce rGO and simultaneously provides carboxyl groups for hydrogen bonding in the three-dimensional self-assembly of aerogel. It is also proven that the as-synthesized rGO aerogel possesses a pseudocapacitive effect, owing to the presence of carboxyl groups. This facile reduction approach by an easily available source successfully produces rGO aerogel with 20-fold charge storage capacity enhancement (121 F/g at 0.4 A/g) as compared to the GO. It suggests this facile approach has great potential to construct lightweight graphene aerogel for energy storage applications.

Keywords Green reduction · Gelation · Cola · Functionalization · Supercapacitor

Introduction

A highly ordered structure of graphene known as graphene aerogel has been in the limelight due to its unique structural characteristics. It possesses high porosity, high specific surface area, and high conductivity [1, 2], which facilitates its employment in energy generation [3], regenerative medicine and drug delivery [4, 5], sensors [6], energy storage [7], pollutant removal [8–11], and gas separation [12]. Graphene aerogel can be constructed from precursor graphene oxide by either hydrothermal assistance [13] or gelation/cross-linking [14]. The freeze drying or freeze casting is usually employed after gelation to remove the solvents while fixing the dispersion structure to produce aerogel with high surface area and porosity [15–18]. Graphene oxide (GO) is commonly being used as the precursor for graphene-based aerogel due to its high elasticity, flexibility, and stable colloidal dispersions formation ability that can be converted into reduced graphene oxide (rGO) [19, 20]. The reduction can be accomplished via common chemical reducing agents such as hydrazine [21] or sodium borohydride [22]. However, using such reducing agents triggers safety as well as environmental issues. Green reducing agents such as vitamin C [23], green tea [24], rose water [25], and other natural compounds [26, 27] have received immense research interest due to their effective reducing capabilities while possessing zero harm to the environment. Tremendous scientific efforts have been introduced to study the eco-friendly approach to produce rGO. In the quest for eco-friendly reduction approach, the availability of reducing agents should be the consideration factor as easily available, and effective reducing agent should be highly preferred.

Herein, we report the easily available soft drink as the reducing agent to reduce GO into rGO. Cola soft drink is used in this work where carbonated water, sugar, phosphoric acid, and caffeine are its major ingredients. The carbonated water in cola soft drink contains carbonic acid that can effectively reduce and functionalize rGO aerogel with carboxyl groups, forming hydrogen bonding between inner sheets and

✉ Kwok Feng Chong
ckfeng@ump.edu.my

1 Faculty of Industrial Sciences and Technology, Universiti Malaysia Pahang, 26300 Gambang, Kuantan, Malaysia

2 Chemistry Department, Faculty of Science, Al−Azhar University, Assiut 71524, Egypt

3 Department of Physics, VIT-AP University, Amaravati, Andhra Pradesh 522237, India

4 Research Centre for Advanced Materials Science (RCAMS), King Khalid University, 9004, Abha 61413, Saudi Arabia

5 Department of Physics, Faculty of Sciences, King Khalid University, 9004, Abha 61413, Saudi Arabia

Published online: 15 July 2021

ultimately leading to rGO aerogel formation. It is further investigated from the electrochemical perspective to assess its energy storage application.

Materials and methods

The GO was prepared using the modified Hummer's method as our previous report [9]. The process includes three main steps, starting with the peroxidation step to get the intercalated graphite compound (GIC), where graphite flake as a precursor of graphene (4 g; + 100 mesh, Graphene Supermarket) was added in a mixture of $K_2S_2O_8$ (6 g), H_2SO_4 (60 mL), and P_2O_5 (6 g) at 80 °C for 6 h. The second step is the washing step until the pH becomes 7 to remove impurities and stop the oxidation step. The last step is to get the full oxidation form of the graphene (Graphene oxide) by incubating the GIC with a mixture of H_2SO_4 solution (300 mL) and$KMnO_4$ (35 g) at 35 °C for 4 h. Deionized water (700) was used to dilute the mixture, and Hydrogen peroxide (H_2O_2 (100 mL) was used to stop the oxidation reaction HCl solution (1:10) is used for washing the GO until pH 7. To get the solid form. In contrast, GO was obtained by suspending graphite oxide in deionized water. An increase in the surface area of GO was obtained by freeze-drying the mixture. To remove the unexfoliated sheets, GO was obtained by suspending graphite oxide in deionized water by centrifugation. The GO aqueous dispersions (8 mg/mL) were prepared and added into 50 mL of cola soft drink (Coca-Cola Classic). Later the solution was heated at 90 °C for 2 h. The black solution turned into a gel suspension, and the formed gel was then washed multiple times with deionized water before subjected to the freeze-drying process. Finally, a free-standing, three-dimensional aerogel (rGO-A) was obtained. Two additional control samples, namely GO@pH 7 and GO@90 °C, were prepared. Under similar experimental conditions, no cola soft drink was added for GO@90 °C; while for the GO@pH 7, the cola soft drink was neutralized by titration to pH 7 before GO was added. The samples were characterized by an infrared spectrometer (PerkinElmer, Spectrum 100), UV–Vis spectrophotometer (Agilent, CARY60), X-ray diffractometer (XRD) (Rigaku, MiniFlex II), Raman spectrometer (Renishaw, inVia Reflex) with 2.33 eV (532 nm) laser energy, and field emission scanning electron microscope (FESEM) (JEOL, JSM7800F) equipped with energy dispersive X-ray spectrometer (EDS). The chemical groups of samples were studied by X-ray photoelectron spectrometer (XPS, PHI 5000 VersaProbe II), with monochromatic Al K_α X-ray source at 117.40 and 29.35 eV for wide and narrow scan, respectively). The electrochemical experiment (AUTOLAB, PGSTAT30) was performed in a 3-electrode system with the sample, platinum wire, and Ag/AgCl as working, counter, and reference electrodes, respectively. All electrochemical experiment was conducted in 5 M KOH aqueous electrolyte.

Results and discussion

The reduction of GO was investigated by UV–Vis spectroscopy (Fig. 1a). The absorption peaks at 230 nm indicate the π-π* transition peak of the aromatic ring, which is prominent in GO, GO@ 90 °C and GO@pH 7. Additionally, the broad shoulder peaks (300 nm) attributable to n-π* transition, can be observed for those samples, which indicates the presence of oxygen functionalities. On the other hand, the red-shifting of π-π* transition peak to 270 nm for rGO-A sample signifies the π-conjugation network restoration during the reduction process by soft drink [28]. The oxygen functionalities removal is also supported by the diminishment of the broad shoulder peak at 300 nm. In XRD analysis (Fig. 1b), GO exhibits an intense diffraction peak (002) at $2\theta = 9.82°$, which corresponds to the *d*-spacing of 0.899 nm. A similar XRD pattern is observed for GO@90 °C and GO@pH 7, where diffraction peaks are seen at $2\theta = 9.82°$ and $2\theta = 10.5°$, respectively [29]. It shows an insignificant change of *d*-spacing for both samples. However, the rGO-A exhibits an intense (002) peak shifting to $2\theta = 25.1°$ with a calculated *d*-spacing of 0.351 nm. The decrease of *d*-spacing can be associated with removing oxygen functional groups on GO sheets, indicating the successful reduction of GO by cola soft drink. The observed peak broadening in rGO-A could be due to the structural nonuniformity [30]. The additional diffraction peak for rGO-A at $2\theta = 43.0°$ shows (100) plane of rGO-A layers. Fourier transform infrared spectroscopy (FTIR) (Fig. 1c) was utilized to examine the functional groups changes upon reduction by cola soft drink. It is clearly seen that GO, GO@90 °C and GO@pH 7 demonstrate similar oxygen functional groups related peaks at ca. 1724, 3440, 1220, and 1050 cm^{-1}, which can be attributed to the C=O stretching (carboxyl and carbonyl groups) [31], O–H stretching, epoxy, and sp^2 C–O stretching, respectively [23, 32]. The characteristic peaks of carbon materials can be seen at ca. 1620 cm^{-1} for aromatic sp^2 C=C stretching and ca. 1401 cm^{-1} for C–H bending. Upon reduction by cola soft drink, it can be clearly seen that the intensities of all oxygen functional groups related peaks decreases, with the diminishment of the epoxy group related peak. The intensity for C-H bending peak at ca. 1401 cm^{-1} increases for rGO-A, indicating more reduction of oxygen functional groups into aromatic C–H bonds. The O–H functional group at 3440 cm^{-1} remains for rGO-A, most probably due to the presence of carbonic acid in rGO-A.

Raman spectroscopy is useful for studying the sp^3 and sp^2 disorder in carbonaceous materials, and it is often used to determine the rGO formation [33, 34]. The

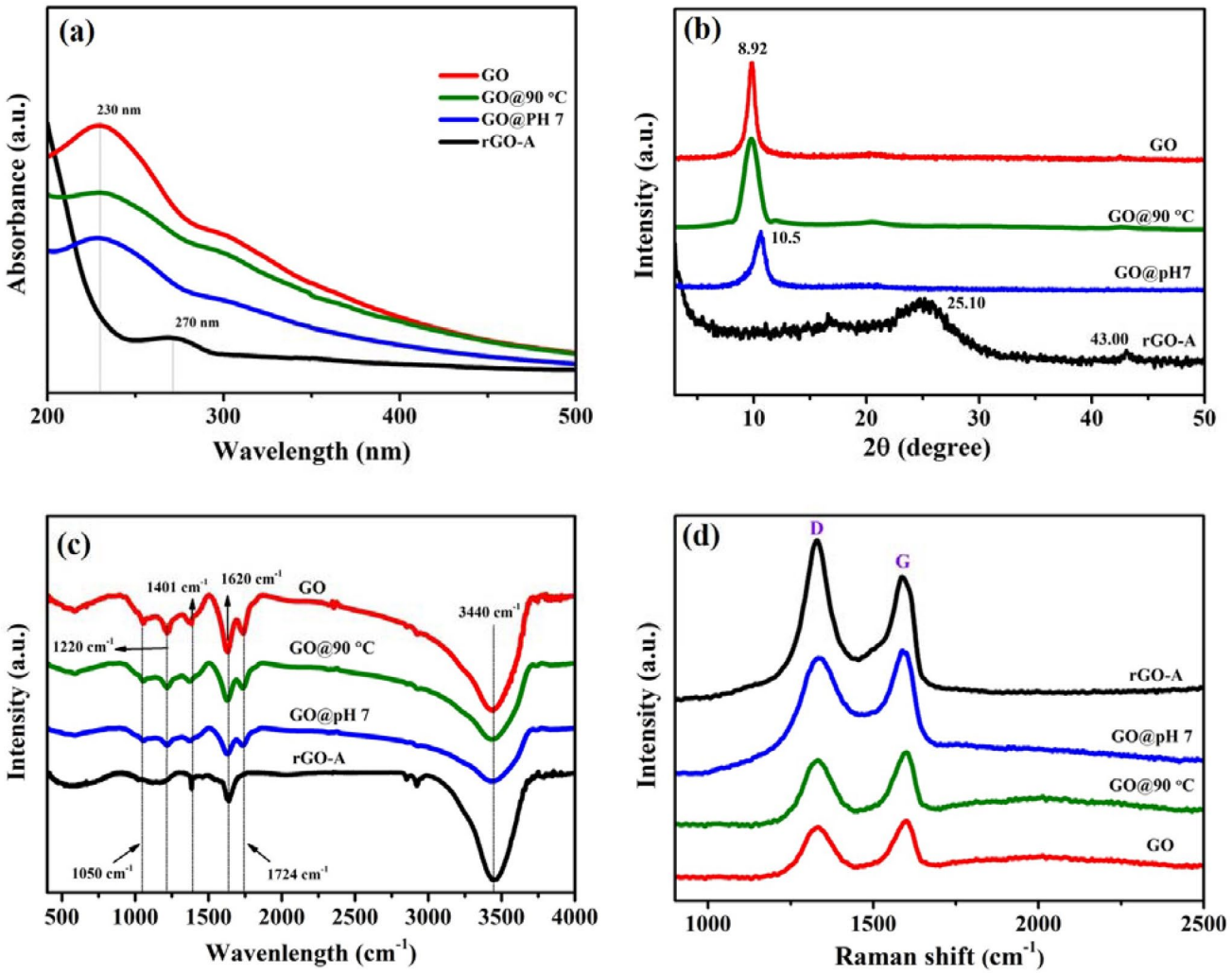

Fig. 1 **a** UV spectra show the red-shifting of π-π* from 230 nm (GO) to 270 nm (rGO-A); **b** XRD patterns show the interlayer spacing decrease of rGO-A; **c** FTIR spectra show the diminishment of oxygen functional groups in rGO-A; **d** Raman spectra show the increased I_D/I_G upon reduction into rGO-A

distinctive feature for carbon samples is the D band and G band, where the former represents the breathing mode of κ-point phonons of A_{1g} symmetry while the latter indicates the first-order scattering of E_{2g} phonon of sp^2 carbon atoms. The D and G peaks (ID/IG) ratio could provide information on the distance between defect sites, and I_D/I_G increases with the mean distance increment between two defects. All the samples demonstrate typical D and G bands in Raman spectra as Fig. 1d. By computing I_D/I_G ratio, it can be seen that GO, GO@90 °C and GO@pH 7 do not exhibit significant variation in I_D/I_G, where I_D/I_G for GO, GO@90 °C and GO@pH 7 are 0.84, 0.91 and 0.94, respectively. However, the rGO-A shows I_D/I_G of 1.23, to indicate the lower defect sites [35]. The oxidation process in GO synthesis generally produces higher defect sites, which can be seen from the lower I_D/I_G ratio. Upon reduction to remove oxygen groups, the sp^2 carbon network is restored with lower defect sites, seen from higher I_D/I_G for rGO-A [36, 37].

The XPS characterization investigates the chemical groups changes in GO and rGO-A. Figure 2a displays the XPS survey scan spectra for GO and rGO-A samples. It is observed that an increase in the C1s peak and a decrease in the O1s for rGO-A compared to that for GO, indicating the deoxygenation in rGO-A. This is further supported by C1s narrow scan (Fig. 2b, c) where the intensity for deconvoluted C−O peak is lower in rGO-A) than that for GO. The diminishment of epoxy-related peak in rGO-A from FTIR analysis also corroborates this claim.

All the physicochemical characterizations suggest successfully reducing GO by cola soft drink into rGO-A in the aerogel form. Both control samples GO@90 °C and GO@pH 7 remain as powder form to indicate the insignificant reduction process. In the absence of cola soft drink, the

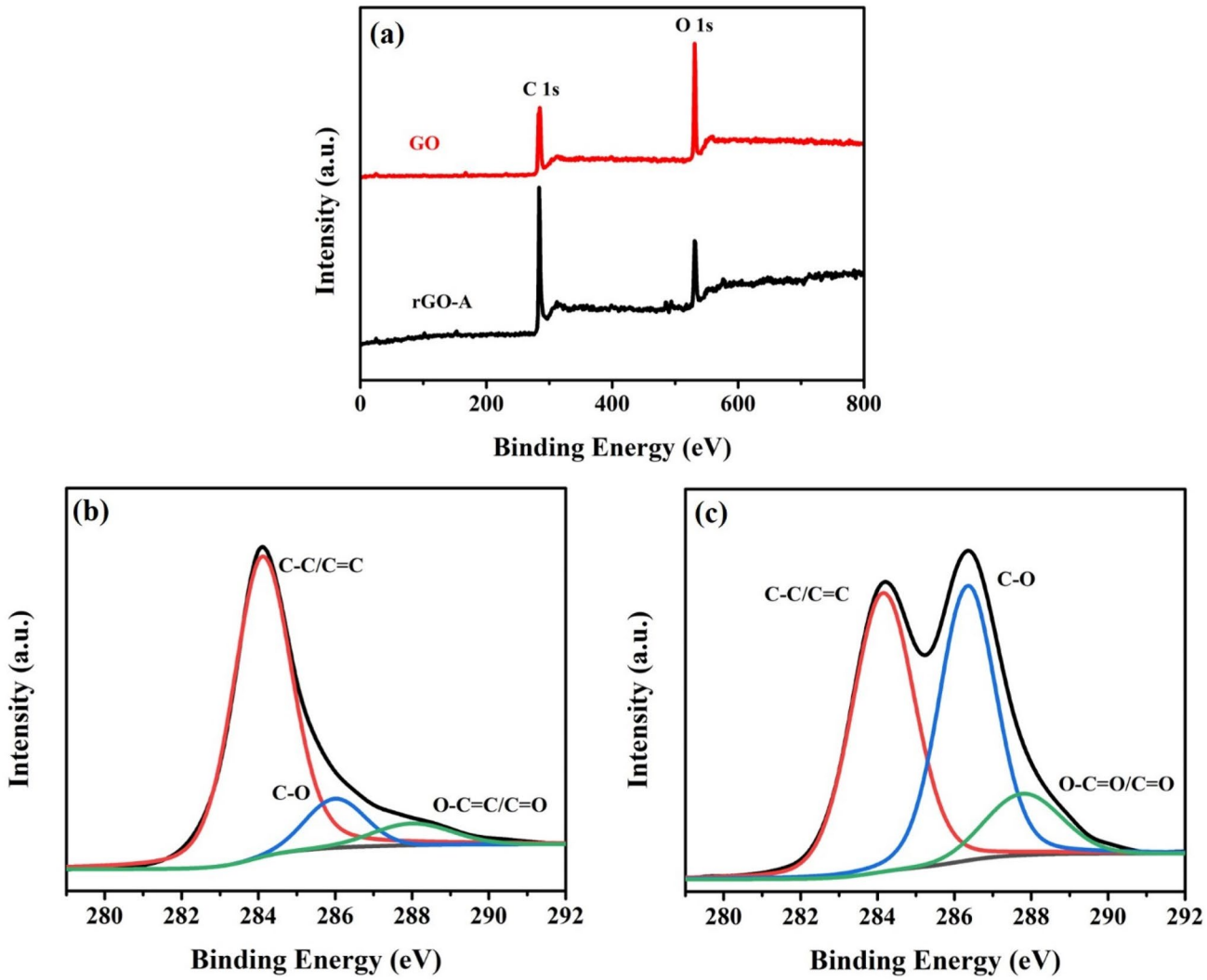

Fig. 2 **a** XPS survey scans spectra of GO and rGO; XPS narrow scan C1s spectra of **b** rGO-A **c** GO

control samples GO@90 °C is unable to reduce GO and proves that the cola soft drink predominantly causes the reduction process in rGO-A. Furthermore, control sample GO@pH 7 also suggests that the reduction process in rGO-A is originated from the acidic compound in cola soft drink as its neutralization at pH 7 could stop the reduction process. Carbon dioxide is typically used in cola soft drinks to create the effervescent effect, and it is converted into carbonic acid (H_2CO_3) upon reaction with water molecules. The mechanism of GO reduction by carbonic acid is proposed to occur via E1, E2, and E1CB reactions (Scheme 1). It can be seen that most of the oxygen functional groups are forcefully removed by carbonic acid. However, the carboxyl groups remain, and the carbonyl groups are converted into carboxyl groups upon reaction with carbonic acid. These are consistent with the FTIR findings to show the remaining oxygen functionalities as carboxyl and hydroxyl groups. Such findings also suggest that the carbonic acid in cola soft drinks not only reduces GO into rGO-A; it simultaneously functionalizes rGO-A with a carboxyl group. The presence of the carboxyl group provides the hydrogen bonding interaction among rGO-A sheets to form the gelation of 3D network. Upon freeze-drying, the lightweight rGO-A is presented as aerogel, which can be supported by the cotton wool as illustrated in Scheme 1. The lightweight rGO-A can be associated with its unique morphology. The role of carbonic acid in GO reduction has been demonstrated by Wadekar et al. [38]. However, other constituents in cola soft drink such as sugar could assist in aerogel formation in our work. It has been reported that sugar could stabilize and increase the rate of the gelation process [39, 40]. The strong hydrated sugar molecule is found to reduce water surrounding the carboxyl functionalized rGO sheets, thus promoting inter sheets hydrogen bonding to form aerogel [41, 42].

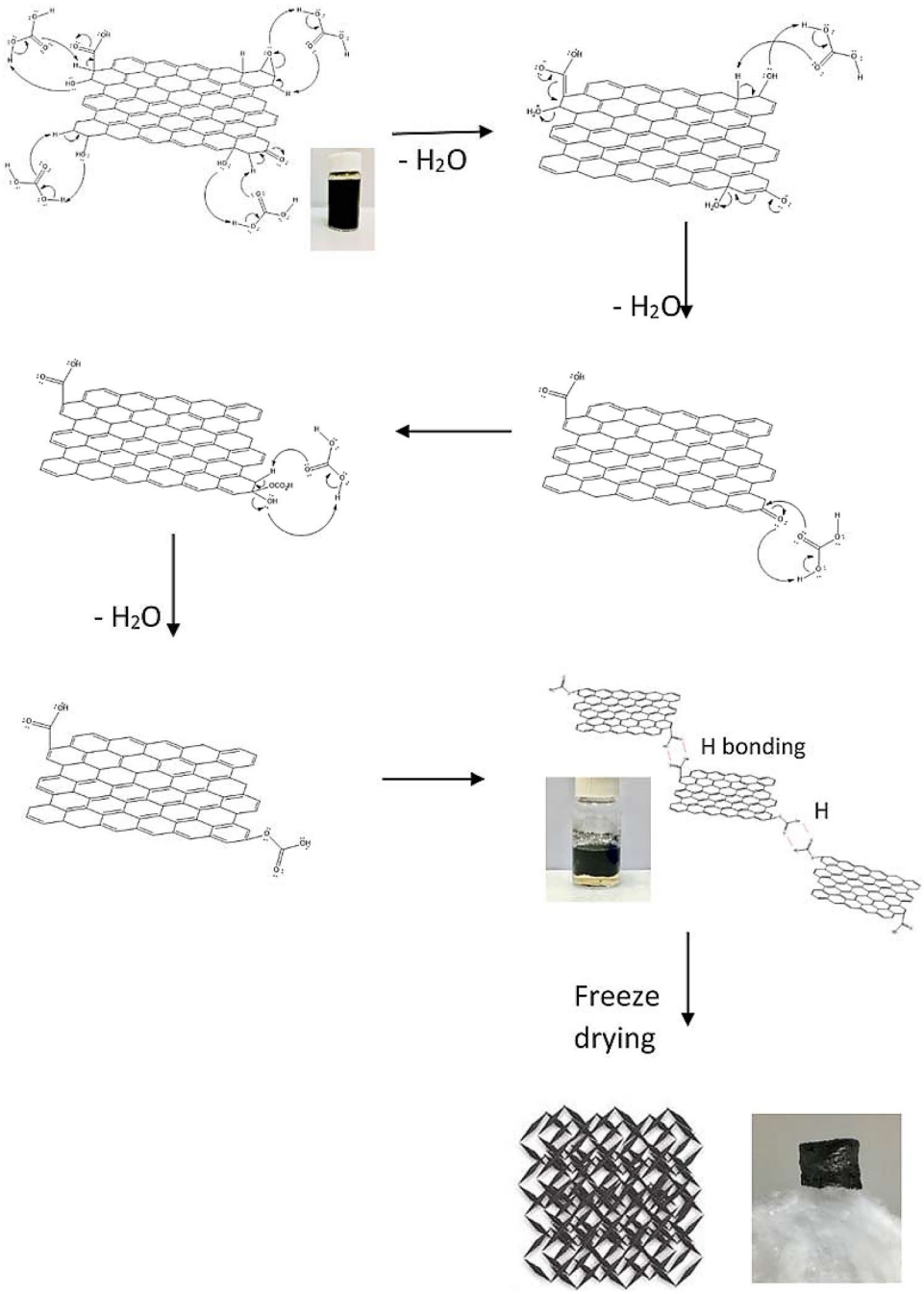

Scheme 1 Simultaneous reduction and functionalization of rGO aerogel by carbonic acid via E1, E2, and E1CB reactions

In Fig. 3a, FESEM image of rGO-A shows the 3D interconnected network constructed by rGO-A sheets randomly orientation. This interconnected network renders rGO-A to be highly porous, which corroborates its lightweight behavior. The functionalized carboxyl group plays a vital role in connecting rGO-A sheets via hydrogen bonding during aerogel formation. In contrast, the prior GO reduction (Fig. 3b) shows a compact structure, which may limit its usage in surface-area-dependent applications such as supercapacitor. Elemental analysis (Table 1) reveals that the C/O ratio increases from 1.80 (GO) to 3.82 (rGO-A) upon reduction by cola soft drink. It shows the successful GO reduction by cola soft drink. The oxygen functional groups at GO act as the spacer to prevent the interlayer stacking and their removal in rGO-A causes the decrease in interlayer spacing, as seen from lower *d*-spacing in rGO-A (in XRD analysis). The remaining 20.74% of oxygen content in rGO-A can be attributed to the oxygen atoms from the carboxyl group that is functionalized on rGO-A. The EDS spectra for GO and rGO-A are shown as Fig. 3c, d, respectively.

The electrochemical performance of the rGO-A was further studied using a three-electrode configuration in

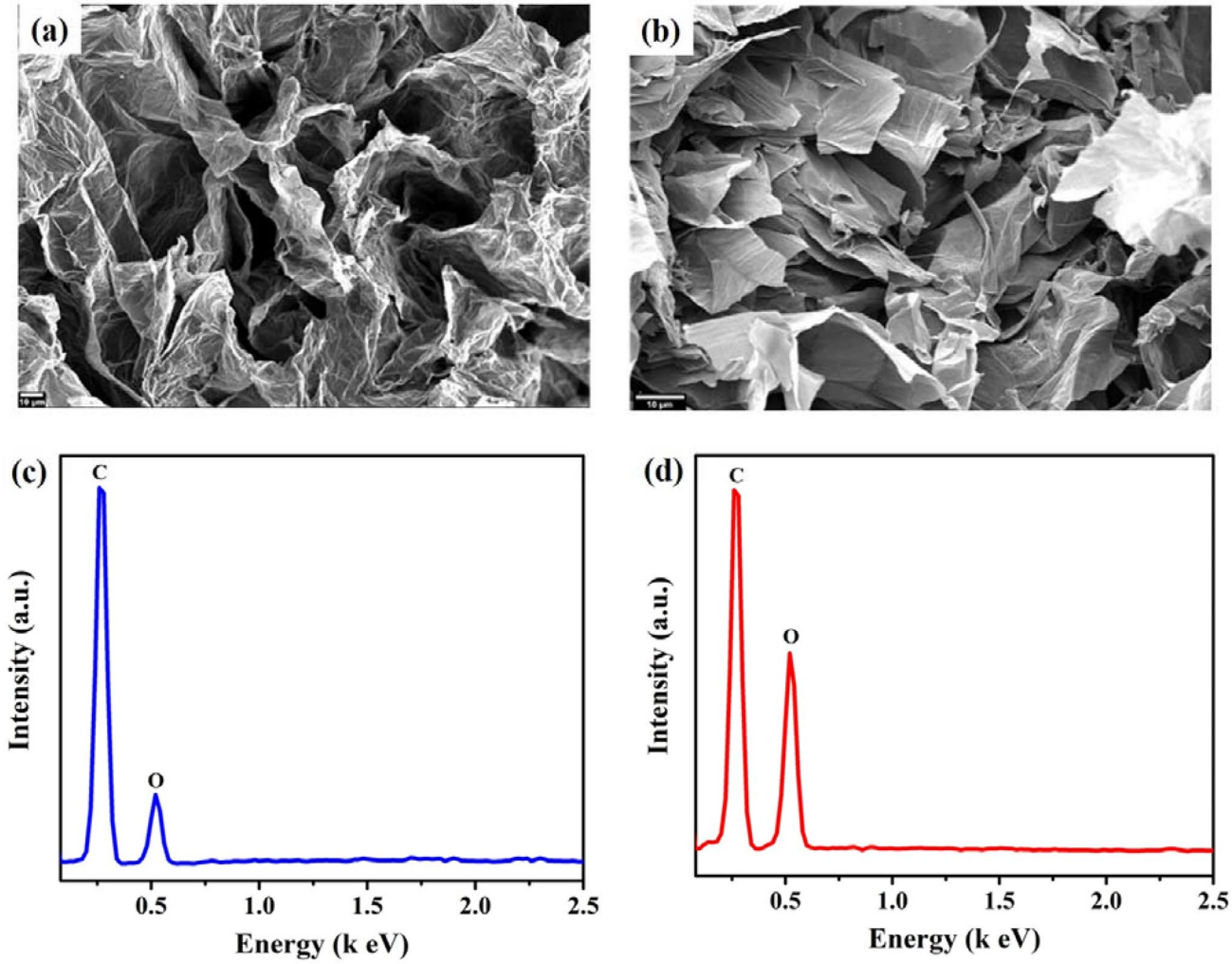

Fig. 3 FESEM images show **a** interconnected sheets network of rGO-A aerogel; **b** compact sheets of GO. EDS analysis for **c** rGO-A and **d** GO

Table 1 EDS detailed content of carbon and oxygen, including C/O ratio for GO and rGO-A

Sample	C	O	C/O ratio
GO	64.08%	35.92%	1.80
rGO-A	79.26%	20.74%	3.82

5 M KOH. The applied potential range was optimized by checking cyclic voltammetry (CV) at different ranges, as shown in Fig. 4a. The optimum working potential range was determined by observing the gas evolution [43], where the rGO-A electrode functions at a potential range from − 1 to 0 V, without any gas evolution. Gas bubbles can be found at the electrode surface from − 1.0 to 0.1 V, which can be seen from the sharp increase of current at 0.1 V. The CV curves for rGO-A and GO electrodes are shown in Fig. 4b and c, respectively. It can be seen that both electrodes at different scan rates exhibit quasi-rectangular CV curves, a clear sign of electrical double layer capacitance (EDLC) [44–47]. Additionally, both rGO-A and GO electrodes show small redox peaks, which can be inferred from the redox reaction of oxygen functional groups. It shows that the carboxyl group on the rGO-A is contributing to the redox reaction. Figure 4d compares the CV curves of rGO-A and GO electrodes at 75 mV/s scan rate. The larger area under the CV curve for rGO-A electrode indicates a higher EDLC effect than that for GO electrode, which hints at better charge storage capability. The galvanostatic charge–discharge (GCD) was used to investigate the electrode performance under practical application of current load. The GCD curves for rGO-A and GO electrodes at different current loads are shown in Fig. 5a and b, respectively. Both electrodes show identical GCD shapes, with the rGO-A electrode exhibiting longer charging and discharging time under similar current loads than that of GO electrode (Fig. 5c). The specific

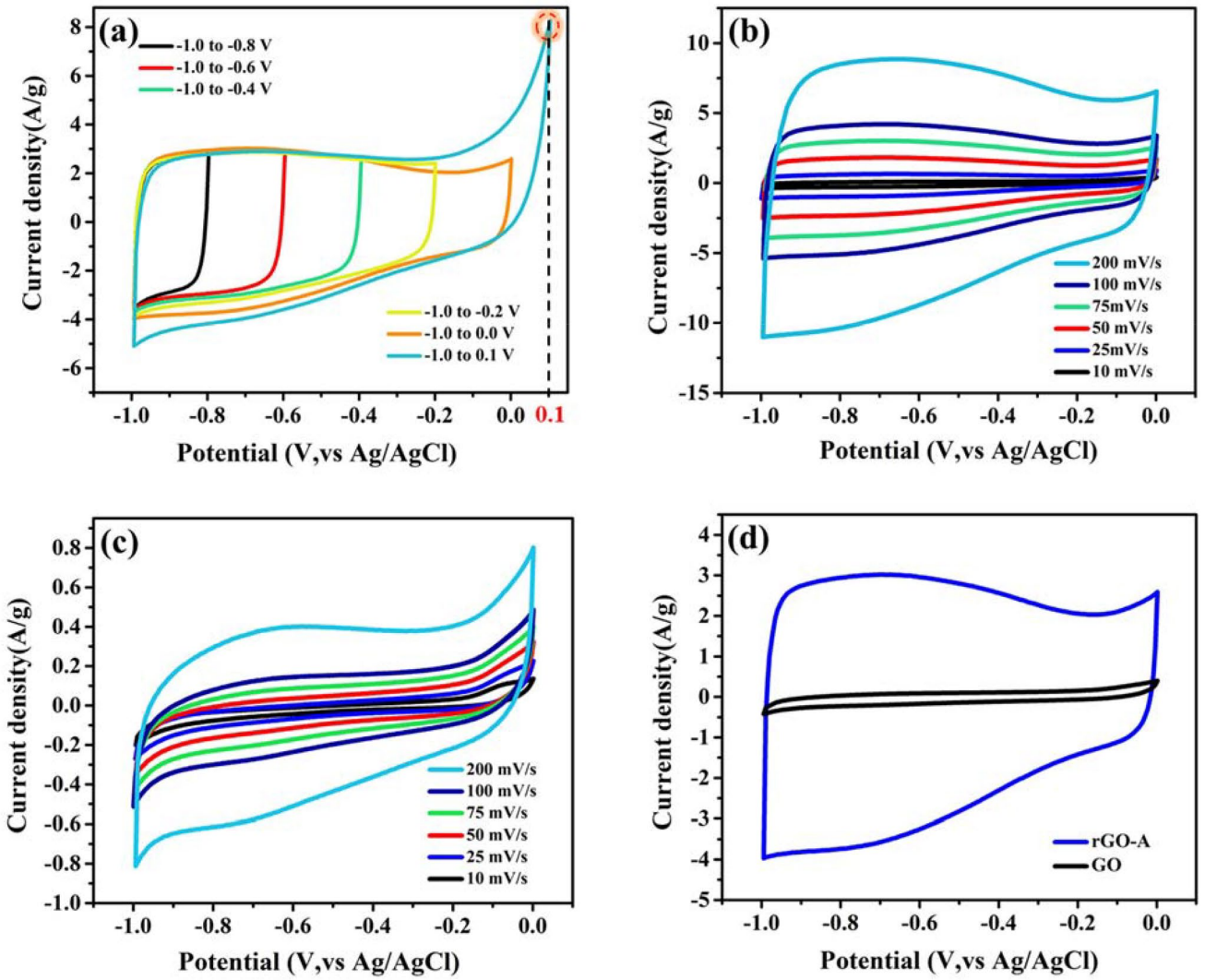

Fig. 4 Cyclic voltammetry curves for **a** rGO-A electrode under potential optimization at 75 mV/s scan rate; **b** rGO-A electrode at different scan rates; **c** GO at different scan rates, and **d** a comparison between GO and rGO-A in 75 mV/s scan rate

capacitance values are calculated from the slope of the discharge curve [48–51] and summarized in Fig. 5d. It can be seen that the GO electrode obtains low charge storage by showing low specific capacitance of ca. 6 F/g at various current densities. Upon reduction by cola soft drink, the rGO-A electrode demonstrates enhanced charge storage with the highest specific capacitance of 121 at 0.4 A/g, an overwhelming value compared to that of GO electrode. The obtained specific capacitance value can be considered as an enhancement of the current reported graphene aerogel-based supercapacitor. For instance, nano-iron oxide (Fe_2O_3)/three-dimensional graphene aerogel (Fe_2O_3/GA) composite shows only 81.3 F g^{-1} in 0.5 M in aqueous solution of Na_2SO_4 [52]. Another interesting note is the increasing specific capacitance of the rGO-A electrode at a lower current density. We could attribute this trend to the enhanced electroactive surface area in the rGO-A electrode, where electrolyte ions could have a longer diffusion time within the electrode structure, contributing to higher ions adsorption.

The electrode kinetics were studied by using electrochemical impedance spectroscopy (EIS) at open circuit potential in a frequency range from 100 to 0.01 Hz with 10 mV amplitude, as shown in Fig. 6a. The EIS fitted data is tabulated in Table 2. The charge transfer resistance (R_{CT}) value for the rGO-A electrode decreases as compared to that for the GO electrode. It clearly proves that cola soft drink removes oxygen functional groups on GO and restores the conductivity network of graphene sheets in rGO-A, allowing easier charge transfer across the electrode/electrolyte interface. The slight increase of Rs value for the rGO-A electrode could be attributed to its electrode preparation, where the rGO-A in aerogel form

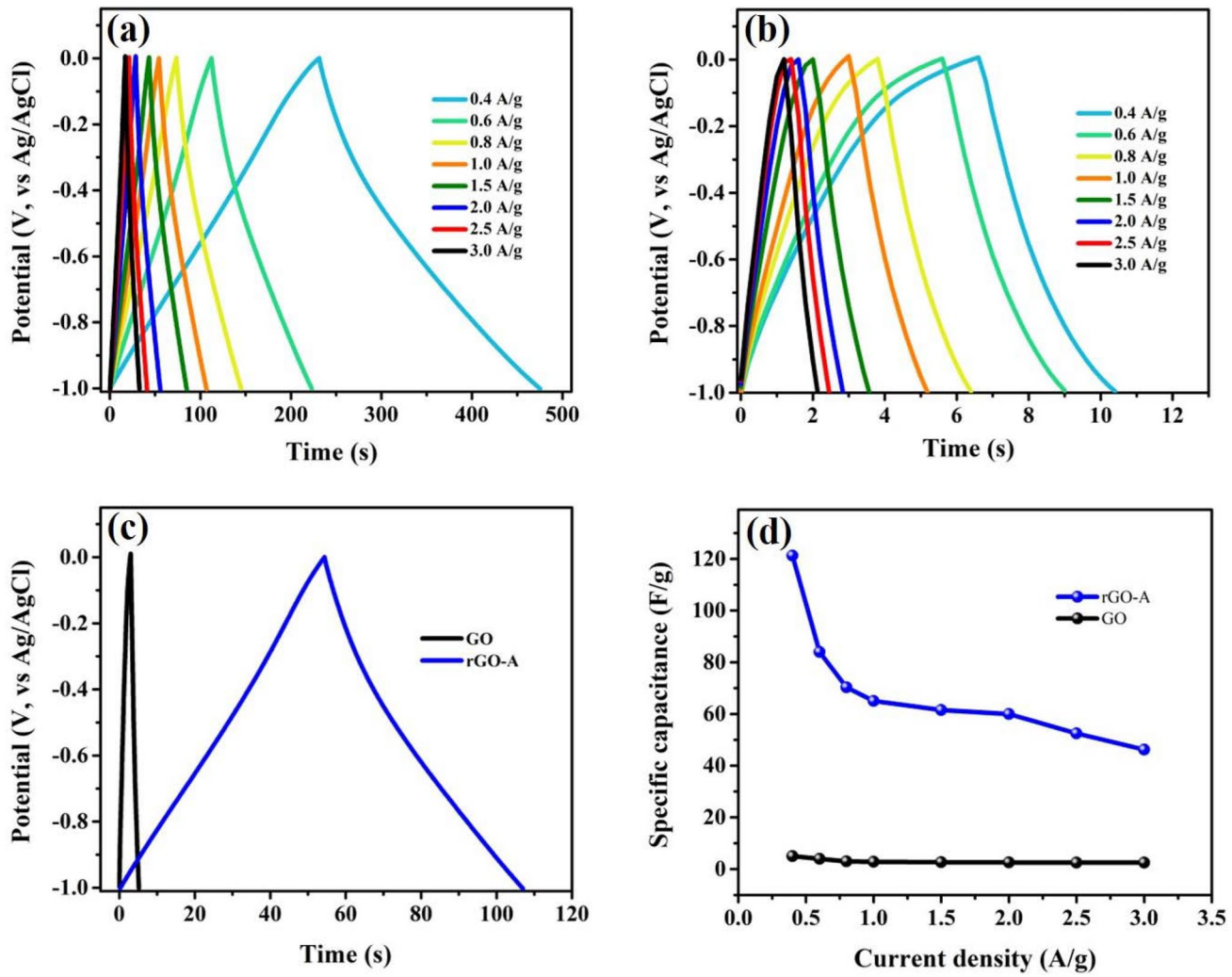

Fig. 5 Galvanostatic charge–discharge curves for **a** rGO-A electrode; **b** GO electrode in a potential window of (− 1 to 0 V) at different current densities; **c** A comparison between GO and rGO-A electrodes at 1 A/g; **d** The calculated specific capacitance of GO and rGO-A electrodes at different current densities in 5 M KOH

was directly used as the working electrode. Meanwhile, additives (binder and conducting carbon) were added to the powdery GO during its electrode preparation. The near-vertical line at the low-frequency region for the rGO-A electrode could be attributed to the aerogel nature of rGO-A, which allows more ions adsorption for capacitive behavior. This is also supported by the low Warburg diffusion (W) resistance. As seen in CV and GCD findings, the charge storage enhancement in the rGO-A electrode is mainly due to the higher electroactive surface area of the aerogel structure and functionalized carboxyl groups. This is further validated in the EIS by calculating electroactive surface area (S_E) from the equation $S_E = C_{dm}/C_d$ [49, 53, 54], where, $C_{dm} = (2\pi fmZ'')^{-1}$, Z" is the imaginary impedance from Nyquist plots at the frequency of 0.01 Hz and C_d is a constant value of 20 μF/cm^2 for carbonaceous materials [55]. The S_E value for rGO-A electrode in 5 M KOH is 764.52 m^2/g as compared to 164.86 m^2/g for GO electrode.

Lastly, the rGO-A electrode's stability was investigated by GCD tests up to 10,000 GCD cycles (Fig. 6b). Electrode with high capacitance retention is crucial for continuous usage for the supercapacitor and the rGO-A electrode shows high stability with capacitance retention of 93.04% after 10,000 GCD cycles. A comparison GCD curves before and after the stability test is presented as Fig. 6b insets and it shows insignificant change after 10,000 GCD cycles.

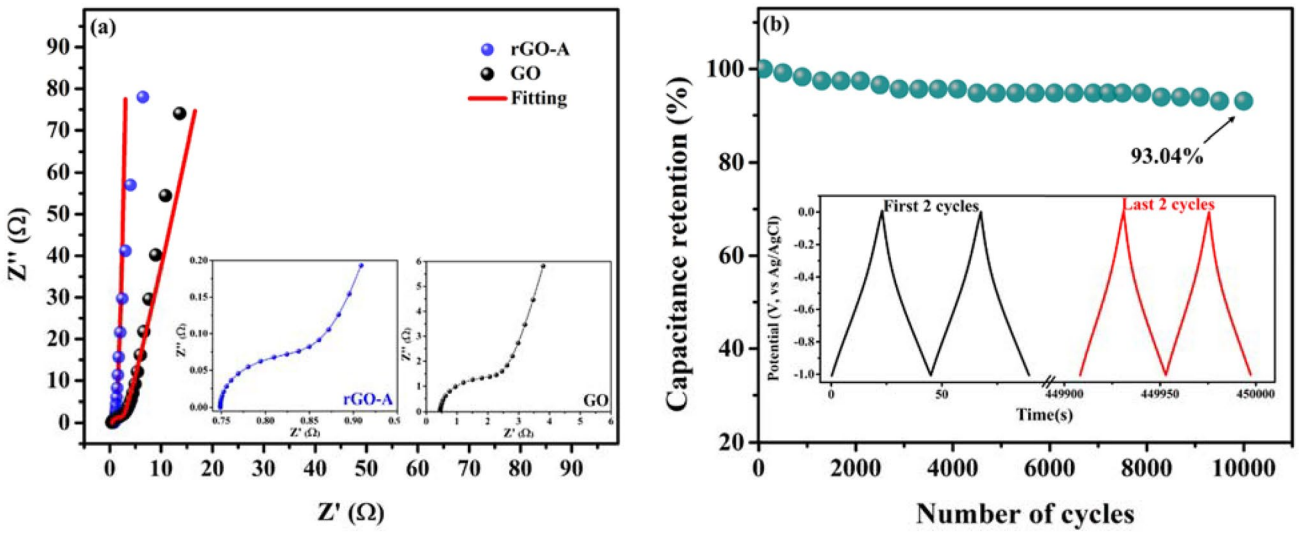

Fig. 6 **a** Nyquist plot of GO and rGO-A electrodes in 5 M KOH, the insets represent the high-frequency regions for GO in black and rGO-A in blue. **b** The cycling stability of rGO-A electrode at 2 A/g for 10,000 cycles, the inset shows GCD curves before and after the stability test

Table 2 The parameters obtained by fitting the experimental impedance data of rGO-A and GO electrodes

	R_S (Ω)	R_{CT} (Ω)	C (mF)	CPE (Ω^{-1} s^n)	S_E (m^2/g)	W (Ω)
rGO-A	0.75	0.10	7.70	0.15	764.52	0.001
GO	0.50	2.00	0.26	0.41	164.86	0.100

Conclusions

In this work, we report a facile approach for simultaneous reduction and functionalization of rGO aerogel using commonly available cola soft drink. The presence of carbonic acid in soft drink removes the oxygen functional groups in GO and provides carboxyl groups for hydrogen bonding between inner sheets. This interconnected network triggers rGO aerogel gelation, and it forms aerogel upon water removal by freeze-drying process. The aerogel structure and functionalized carboxyl group enhance the charge storage of rGO aerogel, which suggests it as the suitable electrode material for supercapacitor. It is anticipated that these findings can stimulate the production of rGO aerogel by using the easily available materials and its application in energy storage.

Acknowledgements The authors would like to acknowledge the funding from the Ministry of Education Malaysia in the form of [RDU1901186:FRGS/1/2019/STG07/UMP/02/6] and Malaysia Toray Science Foundation grant RDU201502. In addition, the authors extend their appreciation to the Deanship of Scientific Research at King Khalid University for funding this work through the research group project under grant number (R.G.P.2/199/42).

References

1. Mao, J., Iocozzia, J., Huang, J., Meng, K., Lai, Y., Lin, Z.: Graphene aerogels for efficient energy storage and conversion. Energy. Environ. Sci. **11**(4), 772–799 (2018)
2. Barrios, E., Fox, D., Li Sip, Y.Y., Catarata, R., Calderon, J.E., Azim, N., Afrin, S., Zhang, Z., Zhai, L.: Nanomaterials in advanced, high-performance aerogel composites: a review. Polymers **11**(4), 726 (2019)
3. Korkmaz, S., Kariper, A.: Aerogel based nanogenerators: Production methods, characterizations and applications. Int. J. Energy. Res. **44**, 11088–11110 (2020)
4. Asha, S., Ananth, A.N., Jose, S.P., Rajan, M.A.J.: Reduced graphene oxide aerogel networks with soft interfacial template for applications in bone tissue regeneration. Appl. Nanosci. **8**(3), 395–405 (2018)
5. Ghawanmeh, A.A., Ali, G.A.M., Algarni, H., Sarkar, S.M., Chong, K.F.: Graphene oxide-based hydrogels as a nanocarrier for anticancer drug delivery. Nano. Res. **12**(5), 973–990 (2019)
6. Ma, Y., Yue, Y., Zhang, H., Cheng, F., Zhao, W., Rao, J., Luo, S., Wang, J., Jiang, X., Liu, Z., Liu, N., Gao, Y.: 3d synergistical mxene/reduced graphene oxide aerogel for a piezoresistive sensor. ACS Nano **12**(4), 3209–3216 (2018)
7. Zhao, X., Li, M., Dong, H., Liu, Y., Hu, H., Cai, Y., Liang, Y., Xiao, Y., Zheng, M.: Interconnected 3D network of graphene-oxide nanosheets decorated with carbon dots for high-performance supercapacitors. Chemsuschem **10**(12), 2626–2634 (2017)

8. Wang, Y., Yadav, S., Heinlein, T., Konjik, V., Breitzke, H., Buntkowsky, G., Schneider, J.J., Zhang, K.: Ultra-light nanocomposite aerogels of bacterial cellulose and reduced graphene oxide for specific absorption and separation of organic liquids. RSC. Adv. **4**(41), 21553 (2014)
9. Lee, S.P., Ali, G.A.M., Algarni, H., Chong, K.F.: Flake size-dependent adsorption of graphene oxide aerogel. J. Mol. Liq. **277**, 175–180 (2019)
10. Liu, H., Mao, Y.: Graphene oxide-based nanomaterials for uranium adsorptive uptake. ES. Mater. Manuf. **13**, 3–22 (2021)
11. Gupta, V.K., Agarwal, S., Sadegh, H., Ali, G.A.M., Bharti, A.K., Hamdy Makhlouf, A.S.: Facile route synthesis of novel graphene oxide-β-cyclodextrin nanocomposite and its application as adsorbent for removal of toxic bisphenol A from the aqueous phase. J. Mol. Liq. **237**, 466–472 (2017)
12. Nidamanuri, N., Li, Y., Li, Q., Dong, M.: Graphene and graphene oxide-based membranes for gas separation. Eng. Sci. **9**(4), 3–16 (2020)
13. Xu, Y., Sheng, K., Li, C., Shi, G.: Self-assembled graphene hydrogel via a one-step hydrothermal process. ACS Nano **4**(7), 4324–4330 (2010)
14. Worsley, M.A., Olson, T.Y., Lee, J.R.I., Willey, T.M., Nielsen, M.H., Roberts, S.K., Pauzauskie, P.J., Biener, J., Satcher, J.H., Baumann, T.F.: High surface area, sp^2-cross-linked three-dimensional graphene monoliths. J. Phys. Chem. Lett. **2**(8), 921–925 (2011)
15. Shao, G., Hanaor, D.A.H., Shen, X., Gurlo, A.: Freeze casting: from low-dimensional building blocks to aligned porous structures—a review of novel materials, methods, and applications. Adv. Mater. **32**, 1907176–1907176 (2020)
16. Cai, J., Tian, J., Gu, H., Guo, Z.: Amino carbon nanotube modified reduced graphene oxide aerogel for oil/water separation. ES Mater. Manuf. **6**(2), 68–74 (2019)
17. Wei, H., Li, A., Kong, D., Li, Z., Cui, D., Li, T., Dong, B., Guo, Z.: Polypyrrole/reduced graphene aerogel film for wearable piezoresisitic sensors with high sensing performances. Adv. Compos. Hybrid Mater. **4**(1), 86–95 (2021)
18. Dong, H., Li, Y., Chai, H., Cao, Y., Chen, X.: Hydrothermal synthesis of $CuCo_2S_4$ nano-structure and N-doped graphene for high-performance aqueous asymmetric supercapacitors. ES. Energy. Environ. **4**(6), 19–26 (2019)
19. Ye, S., Yang, Z., Xu, J., Shang, Z., Xie, J.: Clay-graphene oxide liquid crystals and their aerogels: synthesis, characterization and properties. R. Soc. Open Sci. **6**(2), 181439 (2019)
20. Marina, P.E., Ali, G.A.M., See, L.M., Teo, E.Y.L., Ng, E.-P., Chong, K.F.: In situ growth of redox-active iron-centered nanoparticles on graphene sheets for specific capacitance enhancement. Arabian J. Chem. **12**(8), 3883–3889 (2016)
21. Yan, S., Zhang, G., Li, F., Zhang, L., Wang, S., Zhao, H., Ge, Q., Li, H.: Large-area superelastic graphene aerogels based on a room-temperature reduction self-assembly strategy for sensing and particulate matter (PM25 and PM10) capture. Nanoscale **11**(21), 10372–10380 (2019)
22. Yang, Z.-Z., Zheng, Q.-B., Qiu, H.-X., Li, J., Yang, J.-H.: A simple method for the reduction of graphene oxide by sodium borohydride with $CaCl_2$ as a catalyst. Carbon **86**, 372 (2015)
23. Fernández-Merino, M.J., Guardia, L., Paredes, J., Villar-Rodil, S., Solís-Fernández, P., Martínez-Alonso, A., Tascón, J.: Vitamin C is an ideal substitute for hydrazine in the reduction of graphene oxide suspensions. J. Phys. Chem. C. **114**(14), 6426–6432 (2010)
24. Wang, Y., Shi, Z., Yin, J.: Facile synthesis of soluble graphene via a green reduction of graphene oxide in tea solution and its biocomposites. ACS. Appl. Mater. Interfaces. **3**(4), 1127–1133 (2011)
25. Haghighi, B., Tabrizi, M.A.: Green-synthesis of reduced graphene oxide nanosheets using rose water and a survey on their characteristics and applications. RSC. Adv. **3**(32), 13365 (2013)
26. Kuila, T., Bose, S., Khanra, P., Mishra, A.K., Kim, N.H., Lee, J.H.: A green approach for the reduction of graphene oxide by wild carrot root. Carbon **50**(3), 914–921 (2012)
27. Suresh, D., Udayabhanu, Pavan Kumar, M.A., Nagabhushana, H., Sharma, S.C.: Cinnamon supported facile green reduction of graphene oxide, its dye elimination and antioxidant activities. Mater. Lett. **151**, 93–95 (2015)
28. Kavinkumar, T., Varunkumar, K., Ravikumar, V., Manivannan, S.: Anticancer activity of graphene oxide-reduced graphene oxide-silver nanoparticle composites. J. Colloid. Interface. Sci. **505**, 1125–1133 (2017)
29. Park, S., An, J., Potts, J.R., Velamakanni, A., Murali, S., Ruoff, R.S.: Hydrazine-reduction of graphite-and graphene oxide. Carbon **49**(9), 3019–3023 (2011)
30. Lesiak, B., Stobinski, L., Malolepszy, A., Mazurkiewicz, M., Kövér, L., Tóth, J.: Preparation of graphene oxide and characterisation using electron spectroscopy. J. Electron. Spectrosc. Relat. Phenom. **193**, 92–99 (2014)
31. Korkmaz, S., Tezel, F.M., Kariper, A.: Facile synthesis and characterization of graphene oxide/tungsten oxide thin film supercapacitor for electrochemical energy storage. Phys. E. **116**, 113718–113718 (2020)
32. Si, W., Wu, X., Zhou, J., Guo, F., Zhuo, S., Cui, H., Xing, W.: Reduced graphene oxide aerogel with high-rate supercapacitive performance in aqueous electrolytes. Nanoscale. Res. Lett. **8**(1), 247 (2013)
33. Dresselhaus, M.S., Dresselhaus, G., Saito, R., Jorio, A.: Raman spectroscopy of carbon nanotubes. Phys. Rep. **409**(2), 47–99 (2005)
34. Gu, J., She, J., Yue, Y.: Micro/nanoscale thermal characterization based on spectroscopy techniques. ES. Energy. Environ. **9**(2), 15–27 (2020)
35. Teo, E.Y.L., Ali, G.A.M., Algarni, H., Cheewasedtham, W., Rujiralai, T., Chong, K.F.: One-step production of pyrene-1-boronic acid functionalized graphene for dopamine detection. Mater. Chem. Phys. **231**, 286–291 (2019)
36. Ali, G.A.M., Makhlouf, S.A., Yusoff, M.M., Chong, K.F.: Structural and electrochemical characteristics of graphene nanosheets as supercapacitor electrodes. Rev. Adv. Mater. Sci. **40**(1), 35–43 (2015)
37. Ferrari, A.C., Robertson, J.: Raman spectroscopy of amorphous, nanostructured, diamond–like carbon, and nanodiamond. Philos. Trans. R. Soc. London. Ser. A. **362**(1824), 2477–2512 (2004)
38. Wadekar, P.H., Ahirrao, D.J., Khose, R.V., Pethsangave, D.A., Jha, N., Some, S.: Synthesis of aqueous dispersible reduced graphene oxide by the reduction of graphene oxide in presence of carbonic acid. ChemistrySelect **3**(20), 5630–5638 (2018)
39. Schorsch, C., Jones, M.G., Norton, I.T.: Micellar casein gelation at high sucrose content. J. Dairy. Sci. **85**(12), 3155–3163 (2002)
40. Shimizu, S., Matubayasi, N.: Gelation: the role of sugars and polyols on gelatin and agarose. J. Phys. Chem. B. **118**(46), 13210–13216 (2014)
41. Evageliou, V., Richardson, R.K., Morris, E.R.: Effect of sucrose, glucose and fructose on gelation of oxidised starch. Carbohydr. Polym. **42**(3), 261–272 (2000)
42. Doyle, J.P., Giannouli, P., Martin, E.J., Brooks, M., Morris, E.R.: Effect of sugars, galactose content and chainlength on freeze–thaw gelation of galactomannans. Carbohydr. Polym. **64**(3), 391–401 (2006)
43. Shao, Y., El-Kady, M.F., Sun, J., Li, Y., Zhang, Q., Zhu, M., Wang, H., Dunn, B., Kaner, R.B.: Design and mechanisms of asymmetric supercapacitors. Chem. Rev. **118**(18), 9233–9280 (2018)

44. Patil, S.S., Bhat, T.S., Teli, A.M., Beknalkar, S.A., Dhavale, S.B., Faras, M.M., Karanjkar, M.M., Patil, P.S.: Hybrid solid state supercapacitors (HSSC's) for high energy and power density: an overview. Eng. Sci. **12**, 38–51 (2020)
45. Sayyed, S.G., Mahadik, M.A., Shaikh, A.V., Jang, J.S., Pathan, H.M.: Nano-metal oxide based supercapacitor via electrochemical deposition. ES. Energy. Environ. **3**(4), 25–44 (2019)
46. Li, G., Ji, Y., Zuo, D., Xu, J., Zhang, H.: Carbon electrodes with double conductive networks for high-performance electrical double-layer capacitors. Adv. Compos. Hybrid. Mater. **2**(3), 456–461 (2019)
47. Wang, X., Zeng, X., Cao, D.: Biomass-derived nitrogen-doped porous carbons (NPC) and NPC/polyaniline composites as high performance supercapacitor materials. Eng. Sci. **1**(42), 55–63 (2018)
48. Deokate, R.J.: Chemically deposited $NiCo_2O_4$ thin films for electrochemical study. ES. Mater. Manuf. **11**(2), 16–19 (2020)
49. Ali, G.A.M.: Recycled MnO_2 nanoflowers and graphene nanosheets for low-cost and high performance asymmetric supercapacitor. J. Electron. Mater. **49**, 411–5421 (2020)
50. Tian, Y., Yang, X., Nautiyal, A., Zheng, Y., Guo, Q., Luo, J., Zhang, X.: One-step microwave synthesis of MoS_2/MoO_3@graphite nanocomposite as an excellent electrode material for supercapacitors. Adv. Compos. Hybrid. Mater. **2**(1), 151–161 (2019)
51. Ali, G.A.M., Bakr, Z.H., Safarifard, V., Chong, K.F.: Recycled nanomaterials for energy storage (Supercapacitor) applications. In: Makhlouf, A.S.H., Ali, G.A.M. (eds.) Waste recycling technologies for nanomaterials manufacturing, pp. 175–202. Springer International Publishing, Cham (2021)
52. Korkmaz, S., Kariper, A.: Graphene and graphene oxide based aerogels: synthesis, characteristics and supercapacitor applications. J. Energy. Storage. **27**, 101038–101038 (2020)
53. Ali, G.A.M., Habeeb, O.A., Algarni, H., Chong, K.F.: CaO impregnated highly porous honeycomb activated carbon from agriculture waste: symmetrical supercapacitor study. J. Mater. Sci. **54**, 683–692 (2018)
54. Aboelazm, E.A.A., Mohamed, N., Ali, G.A.M., Makhlouf, A.S.H., Chong, K.F.: Recycling of cobalt oxides electrodes from spent lithium-ion batteries by electrochemical method. In: Makhlouf, A.S.H., Ali, G.A.M. (eds.) Waste recycling technologies for nanomaterials manufacturing, pp. 91–123. Springer International Publishing, Cham (2021)
55. Moseley, P.T., Rand, D.A., Davidson, A., Monahov, B.: Understanding the functions of carbon in the negative active-mass of the lead–acid battery: a review of progress. J. Energy. Storage. **19**, 272–290 (2018)